OPEN ACCESS
Journal of Innovative Optical Health Sciences
Vol. 14, No. 1 (2021) 2140001 (10 pages)

DOI: 10.1142/S1793545821400010

World Scientific
www.worldscientific.com

Identification of oral squamous cell carcinoma in optical coherence tomography images based on texture features

Zihan Yang*, Jianwei Shang†, Chenlu Liu‡, Jun Zhang§ and Yanmei Liang*,¶
*Institute of Modern Optics, Nankai University
Tianjin Key Laboratory of Micro-Scale Optical
Information Science and Technology
Tianjin 300350, P. R. China

†Department of Oral Pathology
Tianjin Stomatological Hospital
Hospital of Stomatology, Nankai University
Tianjin 300041, P. R. China

‡Department of Oral Medicine
Tianjin Stomatological Hospital
Hospital of Stomatology, Nankai University
Tianjin 300041, P. R. China

§Department of Oral-Maxillofacial Surgery
Tianjin Stomatological Hospital
Hospital of Stomatology, Nankai University
Tianjin 300041, P. R. China
¶ymliang@nankai.edu.cn

Received 28 September 2020
Accepted 19 November 2020
Published 16 December 2020

Surgical excision is an effective treatment for oral squamous cell carcinoma (OSCC), but exact intraoperative differentiation OSCC from the normal tissue is the first premise. As a noninvasive imaging technique, optical coherence tomography (OCT) has the nearly same resolution as the histopathological examination, whose images contain rich information to assist surgeons to make clinical decisions. We extracted kinds of texture features from OCT images obtained by a home-made swept-source OCT system in this paper, and studied the identification of OSCC based on different combinations of texture features and machine learning classifiers. It was demonstrated that different combinations had different accuracies, among which the combination of texture features, gray level co-occurrence matrix (GLCM), Laws' texture measures (LM), and center symmetric auto-correlation (CSAC), and SVM as the classifier, had the optimal comprehensive

¶Corresponding author.

identification effect, whose accuracy was 94.1%. It was proven that it is feasible to distinguish OSCC based on texture features in OCT images, and it has great potential in helping surgeons make rapid and accurate decisions in oral clinical practice.

Keywords: Optical coherence tomography; oral squamous cell carcinoma; identification; texture features; machine learning.

1. Introduction

Oral squamous cell carcinoma (OSCC) is one of the most common cancers in head and neck, accounting for approximately 400,000 new cases annually.[1] In spite of the advancement in cancer targeting therapy, its survival rate post intervention is still not ideal.[2] One of the major challenges is to differentiate OSCC from normal tissue accurately. Visual inspection and tissue palpation are the first step in diagnosis.[3] However, they have some limitations. Even though surgeons are trained to recognize morphological features, they are still a subjective assessment. In order to confirm diagnosis, a biopsy or histopathological examination may be performed.[4] While histopathology is still the gold standard diagnostic method, the invasive and time-consuming make this process inconvenient.

To help surgeons improve diagnostic procedures, many methods of auxiliary diagnosis have been sought including ultrasound,[5] fluorescence,[6] hyperspectral imaging,[7] and magnetic resonance imaging (MRI).[8] As a known real-time, noninvasive, and label-free imaging technique, optical coherence tomography (OCT)[9] has been applied in ophthalmology,[10] cardiology,[11] gastroenterology,[12] and dermatology.[13] The resolution, ranging from about 1–20 μm, is superior to those of other conventional imaging methods, enabling it close to histopathological examination. Its ability of "optical biopsy" gives it the potential to reduce the necessity of invasive tissue sampling via biopsy.[14]

OCT has been studied to evaluate a variety of oral diseases for *ex vitro* and *in vivo*, including various inflammatory,[15] benign disorders,[16] and tumors.[17] In addition to visualizing morphological structures,[18–20] quantification of micro-architectural characteristics can be achieved by analyzing OCT images. However, quantitative analyses of oral mucosal diseases based on OCT images were investigated by only a few papers in recent years. The methods based on optical properties were studied, including standard deviation and spatial frequency to diagnose oral mucosal diseases.[21,22] In the previous work, we imaged OSCC and normal oral mucosa, and quantitatively distinguished OSCC with the accuracy of 91.15% by using optical attenuation model.[23]

With the improving acquisition rate of OCT system, high frame rate imaging provides the possibility for surgeons to visualize the lesion area in real time.[24,25] Besides, abundant objective information extracted from OCT images can assist surgeons to make clinical decisions, among which texture features provide quantitative evaluation and auxiliary diagnosis without the prior knowledge for the surgeons. Texture feature-based methods in OCT images have been studied in brain tissue,[26] artery tissue,[27] and skin tissue.[28] Lenz *et al.* employed different algorithms to extract texture features and applied pattern recognition methods to differentiate meningioma, healthy white, and healthy gray matter, and the average accuracy was nearly 98%.[26] Gan *et al.* combined texture analysis to classify tissue compositions within human atria samples in OCT images and the classification algorithm had an average accuracy of 80.41% for identifying adipose, myocardium, fibrotic myocardium, and collagen tissue compositions.[27] Adabi *et al.* demonstrated that automated pattern recognition provided objective information to the clinician to assist in the diagnosis of abnormalities of cutaneous microstructure by extracting optical and textural features from OCT images of healthy and diseased skin.[28]

In this study, OCT images of 14 OSCC patients scanned from a home-made swept source OCT (SS-OCT) system were used to establish data set for automatic identification. Four types of texture features were extracted and four machine learning algorithms were used to evaluate the performances of different combinations of texture features and determine the effectiveness of features. Our research demonstrates that machine learning algorithms based on texture features can effectively distinguish OSCC from normal mucosal tissue and quantitative performance assessment of the algorithms provided

suggestions for the selection of appropriate methods in diagnosis of oral diseases.

2. Materials and Methods

2.1. *Specimen preparation*

Fresh *ex vivo* oral tissues from 14 patients were scanned by our home-made SS-OCT system[23,29,30] at the Tianjin Stomatological Hospital, Tianjin, China. The central wavelength of the SS is 1310 nm. The axial and lateral resolutions of the system are about 14.7 μm and 17 μm in air, respectively. The maximum imaging depth is 5.7 mm in air. The protocol was approved by Ethics Committee of Tianjin Stomatological Hospital. After OCT *ex vivo* scanning, the samples were fixed and stained with H&E, and their slices were evaluated by an experienced pathologist. Finally, the OCT images were compared with the microscopic images.

In our study, volumetric OCT images were obtained from each sample in different directions and positions, in order to compare with histopathological images easily. Sixty-seven three-dimensional (3D) OCT images were totally obtained, and each consisted of 1000 B-scans. 2D OCT images were selected as data set based on the following criteria. First, OCT images need to be matched with the histopathological images. Second, the images collected at the edge of the excised tissue are removed due to poor image quality. Third, in order to ensure the independence of data, the image of adjacent B-scans should be avoided as far as possible. Finally, 2140 OSCC and 1635 normal mucosa OCT images were used to study the tissue identification in this paper.

2.2. *Feature extraction and identification*

Figure 1 gives the flowchart of OCT image processing. Texture features were first extracted from OCT images. A total of four kinds of features were considered based on our previous work.[31,32] They are gray level co-occurrence matrix (GLCM), Laws' texture measures (LM), center symmetric auto-correlation (CSAC), and local binary pattern (LBP). For GLCM, 20 texture features were extracted from the contrast, correlation, energy, homogeneity, and entropy in four different directions (0, 1), (−1, 1), (−1, 0), and (−1, −1). For LM, certain structural features of images were highlighted by convolving with different filter masks. In our study, five 1D convolution kernels were generated including local average ($L5 = [1\ 4\ 6\ 4\ 1]$), edge ($E5 = [-1\ -2\ 0\ 2\ -1]$), spot ($S5 = [-1\ 0\ 2\ 0\ -1]$), wave ($W5 = [-1\ 2\ 0\ -2\ 1]$), and ripple ($R5 = [1\ -4\ 6\ -4\ 1]$). Twelve texture features based on center CSAC which relate to local intensity variations were extracted.[33] For LBP, a histogram was calculated for every image, where each pixel was compared with its surrounding neighbors.

After all texture features were extracted, a principal component analysis (PCA) algorithm was done by calculating the eigenvectors of the covariance matrix of the initial features to reduce feature dimensionality.[34] The principal components were optimized until a variance of at least 95% was reached. In our study, PCA was performed after standardization preprocessing.

After features dimensionality reduction, four classifiers, which have been proved to be effective in many fields,[35–38] were applied to evaluate the identification performance of different texture features combinations, including support vector machine (SVM), K-nearest neighbor (KNN), decision tree (DT), and random forest (RF).

SVM completes the identification of different categories of data by constructing a set of hyperplanes in the feature space.[39] KNN, as one of the most fundamental algorithms, classifies by measuring the distance between different eigenvalues.

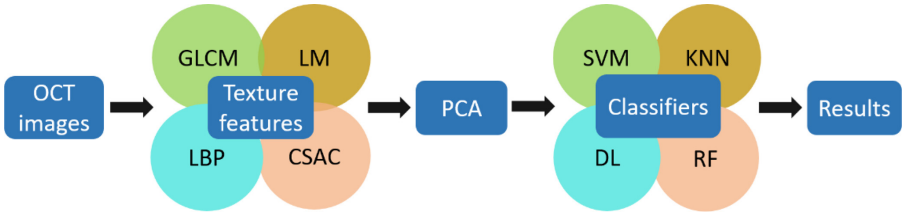

Fig. 1. Flowchart of OCT image processing. GLCM: gray level co-occurrence matrix. LM: Laws' texture measures. LBP: local binary pattern. CSAC: center symmetric auto-correlation. SVM: support vector machine. KNN: K-nearest neighbor. DL: decision tree. RF: random forest. PCA: principal component analysis.

DT is a tree-structured algorithm in which each internal node represents a judgment on an attribute, each branch represents a judgment output, and each leaf represents a category. RF is a classifier based on tree models in which the multiple DTs are used to obtain the accurate final decision.[40]

Finally, the identification results of these four classifiers were analyzed statistically. Moreover, in order to reduce the computational cost and optimize the training results, a 10-fold cross validation was performed. For each tissue, the data set is separated into 10 parts equally. Then, the identification is performed 10 times, where nine parts are used for training and the remaining one part is used for testing each time. The test error is indicated by the following equation:

$$\mathrm{CV}_{(n)} = \frac{1}{n}\sum_{i=1}^{n}\mathrm{Err}_i, \tag{1}$$

where Err_i represents the number of identification errors of the ith model on the ith set of tests.

3. Results

Figure 2 illustrates the OSCC OCT image and its histopathological image. Three 2D images are selected from a 3D image to show the typical structures of OSCC (Fig. 2(a)). Figure 2(b) shows the OCT image of normal oral mucosa, where the epithelial layer (EP) and the lamina propria (LP) can be clearly distinguished, and the basement membrane (BM) is intact, as indicated by a white-dashed curve. In order to show the BM clearly, the white-dashed curve is partly marked in Fig. 2(b). In contrast, the boundary between EP and LP in the OCT image of OSCC is unclear, and BM is destroyed, as shown in Fig. 2(d). In addition, as described in Ref. 29, OSCC is also shown as nested

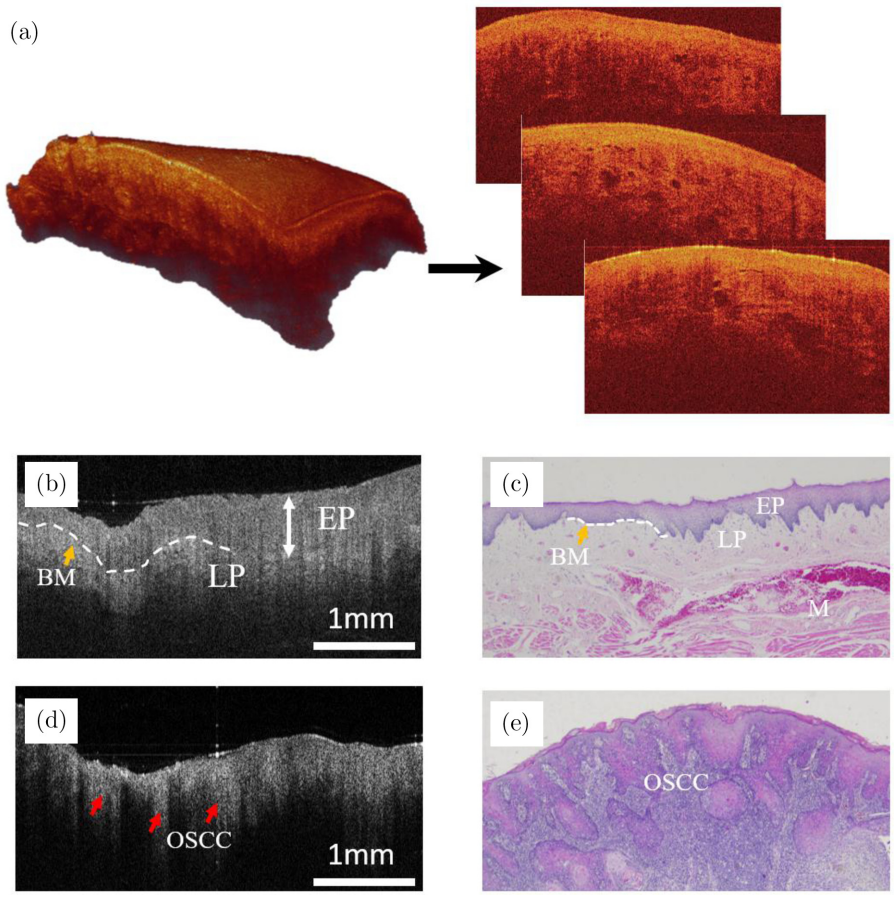

Fig. 2. Typical OCT images of OSCC. (a) is 2D and 3D pseudo color OCT images of OSCC. (b) and (d) are 2D OCT images of the normal oral mucosa and OSCC, respectively. (c) and (e) are the corresponding histopathological images of the normal oral mucosa and OSCC, respectively. EP: epithelial layer, LP: lamina propria, BM: basement membrane, M: muscle, and OSCC: oral squamous cell carcinoma. The scale bar: 1 mm, in both axial and lateral directions.

structures and cord-like structures pointed out by red arrows in Fig. 2(d). The structure of normal mucosa and OSCC are corresponding to their histopathological images, as shown in Figs. 2(c) and 2(e), respectively. The scale bars in Figs. 2(b) and 2(c) are 1 mm, and are the same in both axial and lateral directions.

The formation of OSCC is due to the malignant proliferation of oral squamous epithelial cell, which leads to the formation of solid hard nests in some areas. The hard and dense structures eventually lead to strong scattering of the epithelium and the light cannot penetrate deeper areas. Therefore, comparing Fig. 2(d) with Fig. 2(b), the effective imaging depth of OSCC appears to be small, and some regions form shadows in its OCT image.

Four kinds of texture features were extracted from each image in data set. Fifteen combinations of texture features were used to set up feature vectors. For any combination of the texture features, after PCA was applied, four classifiers were carried out to identify OSCC and their accuracies were calculated, respectively, whose results are shown in Table 1.

As shown in Table 1, we can see the accuracy of a single kind of texture feature with any kinds of classifier is nearly the lowest, which means it is difficult to obtain good identification results for OSCC based on only one kind of texture feature.

Then, we analyzed the combination of all kinds of texture features (GLCM + LM + CSAC + LBP), as shown in Table 1, whose highest accuracy is 93.6% obtained by using SVM classifier. The correlation of their first three principal components in 2D and 3D scatter diagrams are shown in Fig. 3. It can be seen that there are relatively large overlaps among the scatter points for OSCC (red points) and normal tissue (green points), which indicates a risk of overfitting and low robustness by using all of the texture features.

Table 1. Identification accuracies of OSCC with different combinations of texture features and classifiers.

Features \ Classifiers	SVM(%)	KNN(%)	DT(%)	RF(%)
GLCM	92.0	90.5	86.0	82.3
LM	79.3	77.2	75.3	75.8
CSAC	90.2	85.6	81.8	80.7
LBP	78.6	75.7	72.5	76.0
GLCM + LM	93.3	93.4	84.2	84.4
GLCM + CSAC	93.8	88.8	82.2	87.5
GLCM + LBP	93.2	91.2	82.8	85.0
LM + CSAC	92.1	93.2	82.0	90.0
LM + LBP	85.6	81.7	83.4	86.6
CSAC + LBP	91.3	86.1	79.0	84.1
GLCM + LM + CSAC	**94.1**	94.0	86.1	86.4
GLCM + LM + LBP	**94.3**	91.8	87.3	90.0
GLCM + CSAC + LBP	94.0	91.3	81.0	83.7
LM + CSAC + LBP	93.8	91.8	86.9	88.6
GLCM + LM+ CSAC + LBP	93.6	92.6	86.5	86.6

As shown in Table 1, the best accuracy is 94.3%, which was obtained for the combination of GLCM, LM, and LBP and identified by SVM classifier. Figure 4 gives the correlation of their first three principal components in 2D and 3D scatter diagrams, and we can see the scatter points of the first three principal components also have large overlap.

As shown in Table 1, the accuracy of the combination of GLCM, LM, and CSAC is 94.1% by SVM classifier, but according to the scatter diagrams of the correlation of their first three principal components in 2D and 3D scatter diagrams (Fig. 5), there are less overlap among the points of OSCC and the normal tissue than those of Figs. 3 and 4. Therefore, this kind of combination of texture features is more robust.

Based on the above results, it can be concluded that it is not the more texture features, the better the result, and selection of the combination of texture features is important. Moreover, we found that LBP has the lowest accuracy compared to the other three kinds of texture features. For all results, when LBP was employed, large overlap among the points of OSCC and the normal tissue was found. One possible reason is that, as a pixel-wise method, LBP is not appropriate to be used in identifying OSCC in OCT images, even though it usually performs better in other fields.[41,42]

In addition, as shown in Table 1, we found SVM obtained almost all of the best accuracy in the four classifiers for the combination of texture features. In order to further assess its robustness, the grid search of SVM was performed to analyze the effect of different parameters, including the cost parameter c and the width of the Gaussian kernel g, whose results are shown in Fig. 6. The cost parameter c and the width of the Gaussian kernel g are very important parameters of SVM model and affect the generalization ability of the model. The cost parameter c indicates the tolerance of the error, and the choice of g affects the range of Gaussian kernel corresponding to each support vector. By comparing the two results of GLCM + LM + CSAC and

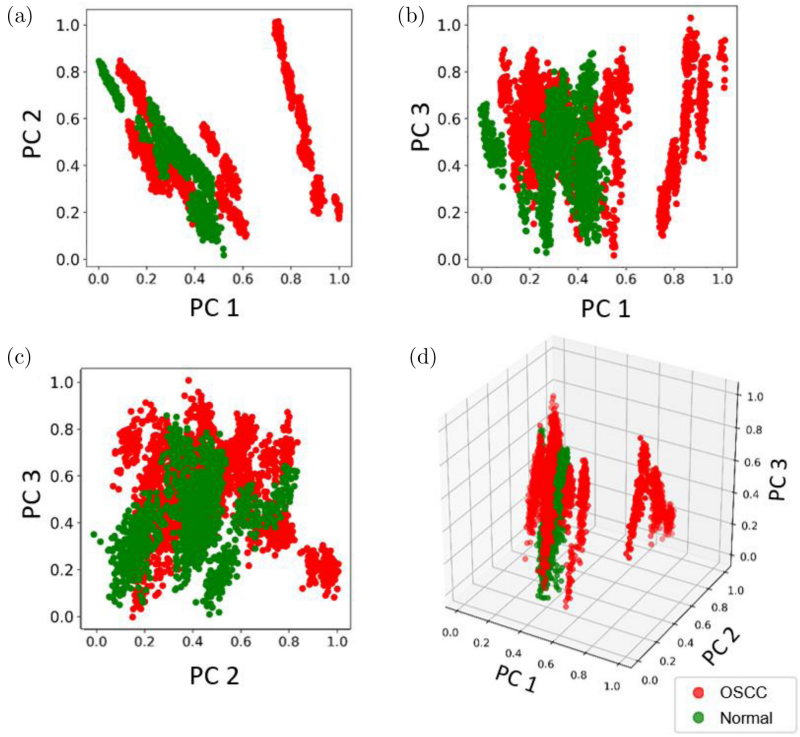

Fig. 3. The scatter diagrams of the first three principal components using PCA for all kinds of texture features. A 2D scatter plot is made for (a) the first principal component (PC1) versus the second principal component (PC2), (b) PC1 versus the third principal component (PC3), (c) PC2 versus PC3, and (d) is a 3D scatter plot for all the three components. OSCC samples are depicted in red points and the normal tissues are green points.

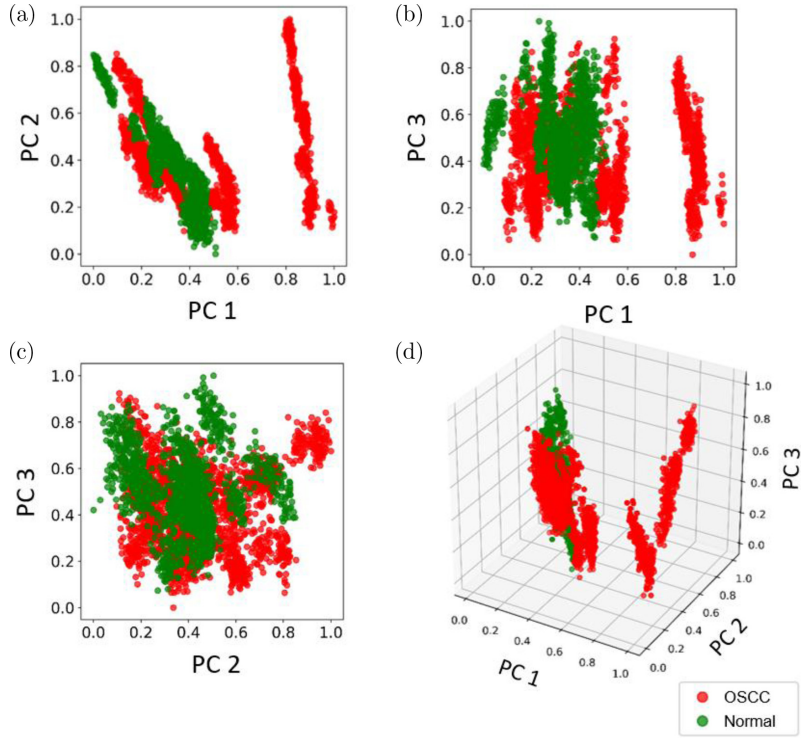

Fig. 4. The scatter diagrams of the first three principal components for the combination of GLCM, LM, and LBP. (a) is the 2D scatter plot for PC1 versus PC2, (b) is the scatter plot for PC1 versus PC3, (c) is PC2 versus PC3, and (d) is a 3D scatter plot for all the three components. OSCC samples are red points, and the normal tissues are green points.

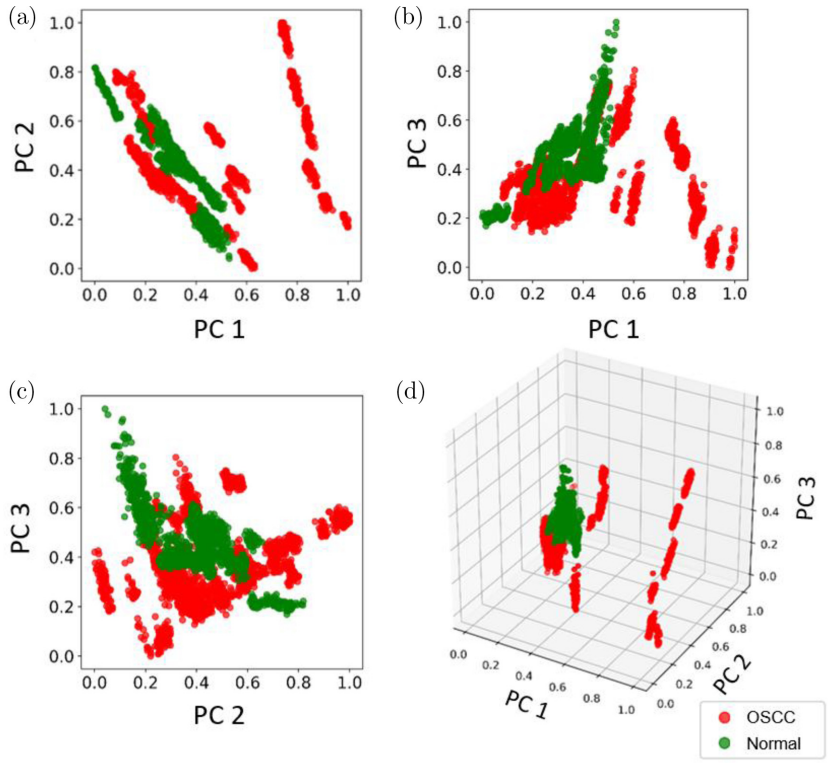

Fig. 5. The scatter diagrams of the first three principal components using PCA for the classification result with the combination of GLCM, LM, and CSAC. A 2D scatter plot is made for (a) PC1 versus PC2, (b) PC1 versus PC3, (c) PC2 versus PC3, and (d) is a 3D scatter plot for all the three components. OSCC samples are red points and the normal tissues are green points.

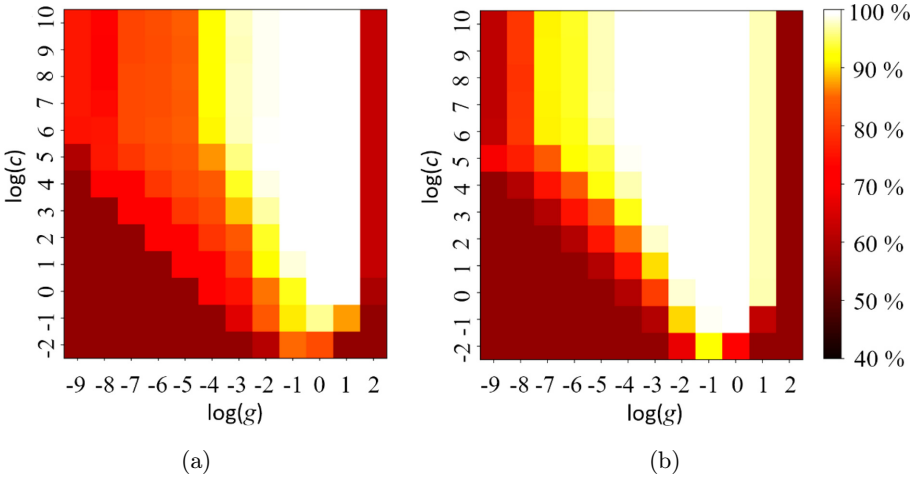

Fig. 6. The results of the grid search of SVM (a) for the GLCM + LM + LBP, and (b) for the GLCM + LM + CSAC. The cost parameter c and the width of the kernel g are displayed in a logarithm scale.

GLCM + LM + LBP combinations, it can be seen that the combination of GLCM, LM, and CSAC has a larger area with an accuracy greater than 90%, which indicates this feature combination and SVM classifier has high robustness for distinguishing OSCC from the normal oral tissue.

4. Discussions

By the combination of texture features and machine learning algorithms, different groups of texture features were evaluated by using four classifiers to distinguish OSCC from the normal oral mucosa in OCT images, whose results proved that different

combinations of texture features and classifiers had different accuracies. Among them, the accuracy obtained by using a single kind of texture feature was low, which was consistent with the conclusion that the image information extracted with only a single kind of texture is inadequate. The combination of GLCM, LM, and LBP had the best accuracy by SVM classifier. However, the robustness was low because of high overlap among the principal components. The combination of GLCM, LM, and CSAC had the optimal comprehensive result.

For the four classification algorithms, SVM obtained the highest accuracy for nearly all kinds of feature combinations, which demonstrated that SVM had the best identification ability for OSCC.

For clinical application, the algorithm processing time is important as accuracy in diagnosing diseases. For image classification, training of classifiers can be carried out offline. For a trained classifier, the processing time of the algorithm is mainly determined by extracting the texture features of the image. The algorithm processing time for extracting different texture features was evaluated, and the average processing time of GLCM, LM, CSAC, and LBP was 0.443 s, 0.215 s, 0.208 s, and 1.232 s, respectively. On the whole, the processing time of each texture extraction algorithm is acceptable for automatic recognition in clinic. The combination of GLCM, LM, and CSAC has the best comprehensive effect, whose processing time is 0.866 s and identification accuracy is 94.1%.

Compared with our previous work,[23] the quantitative analysis method based on attenuation coefficient achieved the accuracy of 91.15% with the attenuation threshold of $4.7\,\mathrm{mm}^{-1}$, whereas this study based on texture features obtained higher accuracy. We found that optical attenuation model can help to detect the edge between OSCC and normal tissue, on the other hand, it is effective to distinguish OSCC from normal tissue based on texture features. Machine learning algorithms have the advantages of strong computing power and OCT images have rich information to be extracted. We believe by combining the attenuation model with the optical characteristics, the identification performance will be further improved.

Different combinations of texture features and machine learning algorithms were studied to identify OSCC in this paper. In the future, we will investigate other more effective feature combinations, feature extraction and algorithms to further improve the identification accuracy of OSCC.

In addition, our study in this paper is based on texture features of OCT images, which does not require a large amount of data compared to deep learning methods. Several thousand OCT images are sufficient without additional workload. The large amount of data we obtained will be expected to be used in deep learning research in the future.

5. Conclusion

Texture features extracted from OCT images provide abundant information of different tissues and can obtain high identification accuracy when they are used appropriately. It was proven that selection of combination of texture features and machine learning algorithms was important to obtain high identification accuracy of OSCC. More effective feature combinations and robust classifiers should be investigated to further improve its accuracy, and make this kind of method to be used in the diagnosis of oral medicine finally.

Conflict of Interest

All of the authors have no relevant financial interests in this paper and no potential conflicts of interest to disclose.

Acknowledgments

This study was supported by the National Natural Science Foundation of China (No. 61875092), Science and Technology Support Program of Tianjin (17YFZCSY00740), and the Beijing-Tianjin-Hebei Basic Research Cooperation Special Program (19JCZDJC65300), and the Fundamental Research Funds for the Central Universities, Nankai University (63201178).

References

1. A. E. Heidari, S. P. Sunny, B. L. James, T. M. Lam, A. V. Tran, J. Yu, R. D. Ramanjinappa, U. K. P. Birur, A. Suresh, M. A. Kuriakose, Z. Chen, P. Wilder-Smith, "Optical coherence tomography as an oral cancer screening adjunct in a low resource settings," *IEEE J. Sel. Top. Quantum* **25**(1), 7202008 (2019).

2. Z. Hamdoon, W. Jerjes, T. Upile, G. McKenzie, A. Jay, C. Hopper, "Optical coherence tomography in the assessment of suspicious oral lesions: An immediate *ex vivo* study," *Photodiagn. Photodyn.* **10**, 17–27 (2013).
3. O. K. Adegun, P. H. Tomlins, E. Hagi-Pavli, G. McKenzie, K. Piper, D. L. Bader, F. Fortune, "Quantitative analysis of optical coherence tomography and histopathology images of normal and dysplastic oral mucosal tissues," *Lasers Med. Sci.* **27**, 795–804 (2012).
4. D. A. Andreadis, A.-M. Pavlou, P. Panta, Biopsy and oral squamous cell carcinoma histopathology, *Oral Cancer Detection*, pp. 133–151, Springer, Cham (2019).
5. R. Izzetti, G. Fantoni, F. Gelli, L. Faggioni, S. Vitali, M. Gabriele, D. Caramella, "Feasibility of intraoral ultrasonography in the diagnosis of oral soft tissue lesions: A preclinical assessment on an *ex vivo* specimen," *Radiol. Med.* **123**, 135–142 (2018).
6. N. Kanchwala, N. Kumar, S. Gupta, H. Lokhandwala, "Fluorescence spectroscopic study on malignant and premalignant oral mucosa of patients undergoing treatment: An observational prospective study," *Int. J. Surg.* **55**, 87–91 (2018).
7. G. Lu, D. Wang, X. Qin, S. Muller, X. Wang, A. Y. Chen, Z. G. Chen, B. Fei, "Detection and delineation of squamous neoplasia with hyperspectral imaging in a mouse model of tongue carcinogenesis," *J. Biophotonics* **11**, 201700078 (2018).
8. J. Heidkamp, W. L. J. Weijs, A. C. H. van Engen-van Grunsven, I. de Laak-de Vries, M. C. Maas, M. M. Rovers, J. J. Futterer, S. C. A. Steens, R. P. Takes, "Assessment of surgical tumor-free resection margins in fresh squamous-cell carcinoma resection specimens of the tongue using a clinical MRI system," *Head Neck* **42**, 2039–2049 (2020).
9. D. Huang, E. A. Swanson, C. P. Lin, J. S. Schuman, W. G. Stinson, W. Chang, M. R. Hee, T. Flotte, K. Gregory, C. A. Puliafito, J. G. Fujimoto, "Optical coherence tomography," *Science* **254**, 1178–1181 (1991).
10. G. Rebolleda, L. Diez-Alvarez, A. Casado, C. Sanchez-Sanchez, E. de Dompablo, J. J. Gonzalez-Lopez, F. J. Munoz-Negrete, "OCT: New perspectives in neuro-ophthalmology," *Saudi J. Ophthalmol.* **29**, 9–25 (2015).
11. M. Paulo, J. Sandoval, V. Lennie, J. Dutary, M. Medina, N. Gonzalo, P. Jimenez-Quevedo, J. Escaned, C. Banuelos, R. Hernandez, C. Macaya, F. Alfonso, "Combined use of OCT and IVUS in spontaneous coronary artery dissection," *JACC Cardiovasc. Imaging* **6**(7), 830–832 (2013).
12. T. H. Tsai, C. L. Leggett, A. J. Trindade, A. Sethi, A. F. Swager, V. Joshi, J. J. Bergman, H. Mashimo, N. S. Nishioka, E. Namati, "Optical coherence tomography in gastroenterology: A review and future outlook," *J. Biomed. Opt.* **22**(12), 121716 (2017).
13. J. Olsen, J. Holmes, G. B. E. Jemec, "Advances in optical coherence tomography in dermatology-a review," *J. Biomed. Opt.* **23**(4), 040901 (2018).
14. J. G. Fujimoto, C. Pitris, S. A. Boppart, M. E. Brezinski, "Optical coherence tomography: An emerging technology for biomedical imaging and optical biopsy," *Neoplasia* **2**(1), 9–25 (2000).
15. P. Surlin, A. Camen, S. I. Stratul, A. Roman, D. N. Gheorghe, E. Herascu, E. Osiac, I. Rogoveanu, "Optical coherence tomography assessment of gingival epithelium inflammatory status in periodontal — Systemic affected patients," *Ann. Anat.* **219**, 51–56 (2018).
16. W. Jerjes, T. Upile, B. Conn, Z. Hamdoon, C. S. Betz, G. McKenzie, H. Radhi, M. Vourvachis, M. E. Maaytah, A. Sandison, A. Jay, C. Hopper, "*In vitro* examination of suspicious oral lesions using optical coherence tomography," *Br. J. Oral Maxillofac. Surg.* **48**, 18–25 (2010).
17. A. V. Maslennikova, M. A. Sirotkina, A. A. Moiseev, E. S. Finagina, S. Y. Ksenofontov, G. V. Gelikonov, L. A. Matveev, E. B. Kiseleva, V. Y. Zaitsev, E. V. Zagaynova, F. I. Feldchtein, N. D. Gladkova, A. Vitkin, "*In-vivo* longitudinal imaging of microvascular changes in irradiated oral mucosa of radiotherapy cancer patients using optical coherence tomography," *Sci. Rep.* **7**, 16505 (2017).
18. P.-H. Chen, C.-H. Wu, Y.-F. Chen, Y.-C. Yeh, B.-H. Lin, K.-W. Chang, P.-Y. Lai, M.-C. Hou, C.-L. Lu, W.-C. Kuo, "Combination of structural and vascular optical coherence tomography for differentiating oral lesions of mice in different carcinogenesis stages," *Biomed. Opt. Express* **9**(4), 1461–1476 (2018).
19. B. Davoudi, A. Lindenmaier, B. A. Standish, G. Allo, K. Bizheva, A. Vitkin, "Noninvasive *in vivo* structural and vascular imaging of human oral tissues with spectral domain optical coherence tomography," *Biomed. Opt. Express* **3**(5), 826–839 (2012).
20. M.-T. Tsai, Y. Chen, C.-Y. Lee, B.-H. Huang, N. H. Trung, Y.-J. Lee, Y.-L. Wang, "Noninvasive structural and microvascular anatomy of oral mucosae using handheld optical coherence tomography," *Biomed. Opt. Express* **8**(11), 5001–5012 (2017).
21. C.-K. Lee, M.-T. Tsai, H.-C. Lee, H.-M. Chen, C.-P. Chiang, Y.-M. Wang, C.-C. Yang, "Diagnosis of oral submucous fibrosis with optical coherence tomography," *J. Biomed. Opt.* **14**(5), 054008 (2009).
22. M.-T. Tsai, H.-C. Lee, C.-K. Lee, C.-H. Yu, H.-M. Chen, C.-P. Chiang, C.-C. Chang, Y.-M. Wang, C.

C. Yang, "Effective indicators for diagnosis of oral cancer using optical coherence tomography," *Opt. Express* **16**(20), 15847–15862 (2008).
23. Z. Yang, J. Shang, C. Liu, J. Zhang, Y. Liang, "Identification of oral cancer in OCT images based on an optical attenuation model," *Laser Med. Sci.* **35**(9), 1999–2007 (2020).
24. K. Liang, O. O. Ahsen, Z. Wang, H.-C. Lee, W. Liang, B. M. Potsaid, T.-H. Tsai, M. G. Giacomelli, V. Jayaraman, H. Mashimo, X. Li, J. G. Fujimoto, "Endoscopic forward-viewing optical coherence tomography and angiography with MHz swept source," *Opt. Lett.* **42**(16), 3193–3196 (2017).
25. S. Wang, M. Singh, A. L. Lopez III, C. Wu, R. Raghunathan, A. Schill, J. Li, K. V. Larin, I. V. Larina, "Direct four-dimensional structural and functional imaging of cardiovascular dynamics in mouse embryos with 1.5 MHz optical coherence tomography," *Opt. Lett.* **40**(20), 4791–4794 (2015).
26. M. Lenz, R. Krug, C. Dillmann, R. Stroop, N. C. Gerhardt, H. Welp, K. Schmieder, M. R. Hofmann, "Automated differentiation between meningioma and healthy brain tissue based on optical coherence tomography *ex vivo* images using texture features," *J. Biomed. Opt.* **23**(7), 071205 (2018).
27. Y. Gan, D. Tsay, S. B. Amir, C. C. Marboe, C. P. Hendon, "Automated classification of optical coherence tomography images of human atrial tissue," *J. Biomed. Opt.* **21**(10), 101407 (2016).
28. S. Adabi, M. Hosseinzadeh, S. Noei, S. Conforto, S. Daveluy, A. Clayton, D. Mehregan, M. Nasiriavanaki, "Universal *in vivo* textural model for human skin based on optical coherence tomograms," *Sci. Rep.* **7**, 17912 (2017).
29. Z. Yang, J. Shang, C. Liu, J. Zhang, F. Hou, Y. Liang, "Intraoperative imaging of oral-maxillofacial lesions using optical coherence tomography," *J. Innov. Opt. Health Sci.* **13**(2), 2050010 (2020).
30. K. Li, Z. Yang, W. Liang, J. Shang, Y. Liang, S. Wan, "Low-cost, ultracompact handheld optical coherence tomography probe for *in vivo* oral maxillofacial tissue imaging," *J. Biomed. Opt.* **25**(4), 046003 (2020).
31. F. Hou, Y. Yu, Y. Liang, "Automatic identification of parathyroid in optical coherence tomography images," *Laser Surg. Med.* **49**, 305–311 (2017).
32. D. Bian, K. Tao, Z. Yuan, H. Kuang, Z. Liu, Y. Liang, "Identification of atherosclerotic plaques in intravascular optical coherence tomography images based on textures and artificial neural network," *Laser Phys.* **30**, 035602 (2020).
33. X. Qi, M. V. Sivak Jr, G. Isenberg, J. E. Willis, A. M. Rollins, "Computer-aided diagnosis of dysplasia in Barrett's esophagus using endoscopic optical coherence tomography," *J. Biomed. Opt.* **11**(4), 044010 (2006).
34. K. K. Vasan, B. Surendiran, "Dimensionality reduction using principal component analysis for network intrusion detection," *Perspect. Sci.* **8**, 510–512 (2016).
35. Y. Zhu, W. Gao, Z. Guo, Y. Zhou, Y. Zhou, "Liver tissue classification of *en face* images by fractal dimension-based support vector machine," *J. Biophotonics* **13**(4), e201960154 (2020).
36. C. Wang, Y. Long, W. Li, W. Dai, S. Xie, Y. Liu, Y. Zhang, M. Liu, Y. Tian, Q. Li, Y. Duan, "Exploratory study on classification of lung cancer subtypes through a combined K-nearest neighbor classifier in breathomics," *Sci. Rep.* **10**, 5880 (2020).
37. M. Tsai, H. Wang, G. Lee, Y. Lin, S. Chiu, "A decision tree based classifier to analyze human ovarian cancer cDNA microarray datasets," *J. Med. Syst.* **40**(1), 21 (2016).
38. C. He, Z. Li, J. Wang, Y. Huang, Y. Yin, Z. Li, "Atherosclerotic plaque tissue characterization: An OCT-based machine learning algorithm with *ex vivo* validation," *Front. Bioeng. Biotechnol.* **8**, 749 (2020).
39. N. Anantrasirichai, A. Achim, J. E. Morgan, I. Erchova, L. Nicholson, SVM-based texture classification in optical coherence tomography, *IEEE 10th Int. Symp. Biomedical Imaging*, San Francisco, CA, 2013, pp. 1332–1335.
40. A. Subudhi, M. Dash, S. Sabut, "Automated segmentation and classifiaction of brain stoke using expectation-maximization and random forest classifier," *Biocybern. Biomed. Eng.* **40**, 277–289 (2020).
41. J. Xu, W. Yang, C. Wan, J. Shen, "Weakly supervised detection of central serous chorioretinopathy based on local binary patterns and discrete wavelet transform," *Comput. Biol. Med.* **127**, 104056 (2020).
42. Z. Camlica, H. R. Tizhoosh, F. Khalvati, Medical image classification via SVM using LBP features from saliency-based folded data, *The 14th Int. Conf. Machine Learning and Applications (IEEE ICMLA'15)*, Miami, Florida, USA, 2015, pp. 128–132.